1.2 REPEATING PATTERNS OF PRECIPITATION AND SURFACE PRESSURE EVOLUTION IN MIDLATITUDE MESOSCALE CONVECTIVE VORTICES

Eric P. James* and Richard H. Johnson
Colorado State University, Fort Collins, Colorado

1. INTRODUCTION

Mesoscale convective vortices (MCVs) are a commonly observed and well-documented feature of mature to decaying mesoscale convective systems (MCSs) in both the midlatitudes and the tropics. There have been only a few studies investigating the surface features that accompany MCVs; most of these have been based on data from the Oklahoma-Kansas Preliminary Regional Experiment for Storm-Scale Operational and Research Meteorology (OK PRE-STORM; Cunning 1986) during the summer of 1985, which provided the first high-resolution surface observations of MCSs and their associated MCVs.

An investigation of the 23-24 June 1985 OK PRE-STORM MCS by Johnson et al. (1989) found several interesting surface features associated with the decay of the MCS and the development of a midlevel circulation. There was a strong mesohigh situated beneath the stratiform region of the MCS during its mature phase. As the stratiform rain degenerated, this mesohigh rapidly transformed into a strong mesolow. This transformation was coincident with the appearance of a well-defined cyclonic vortex in visible satellite imagery. The authors proposed that the mesolow was the hydrostatic response to warming within a region of strong mesoscale subsidence in the absence of precipitation; this warm subsiding air produced localized “heat bursts” at several mesonet stations.

Brandes (1990) studied the 6-7 May 1985 OK PRE-STORM MCS. He found that the associated MCV focused and intensified a descending rear inflow jet (RIJ) into the southern portion of the system. This subsiding air current led to strong low-level warming and drying at the apex of a well-defined rear inflow notch, producing a mesolow with a perturbation pressure anomaly of -4 hPa. The mesolow within this system was a “wake low”, of the type studied by Johnson and Hamilton (1988). These lows result hydrostatically from concentrated descent within a RIJ; evaporational cooling at the rear of the stratiform region induces subsidence in the jet, which eventually becomes unsaturated and warms adiabatically.

Motivated by the existence of high-resolution surface observations by the Oklahoma Mesonet (OM), this study aims to identify and investigate numerous MCV cases in this region during the warm seasons of 2002-05. We classify the identified MCV cases based on their precipitation and surface pressure evolution, and propose some mechanisms for the frequently-observed mesolows.

2. METHODOLOGY

In this section, we describe our methodology for identifying and analyzing MCV cases, and the basis of our MCV classifications.

2.1. *Case Selection*

We use an automated MCV detection algorithm, developed by Davis et al. (2002; hereafter DAT), to identify cases. This algorithm operates on analyses from the Rapid Update Cycle (RUC; Benjamin et al. 2004) model; details are provided by DAT. The original algorithm operates on the relative vorticity field averaged over the three model levels of 600, 550, and 500 hPa; for this study, the presence of numerous missing levels in the RUC data prompted a modification of the algorithm to search for MCVs based on only one or two of the three model levels if necessary. The algorithm is run on hourly RUC analyses (with 40 km horizontal resolution) during the months of May-August of the years 2002-05. At each time, the algorithm produces a map of relative vorticity maxima that satisfy certain structural criteria (including exceeding a “roundness” threshold and falling below a mesoscale size threshold); these vortices can be tracked between analysis times. For each detected vortex, radar and satellite imagery are examined to determine if the vortex is in fact an MCV. Detected vortices are considered MCVs if they are embedded within, or arise from, significant stratiform precipitation and anvil cloud associated with deep, moist convection. We search for MCVs within a latitude-longitude box containing the state of Oklahoma.

---

* *Corresponding author address:* Eric P. James, Colorado State Univ., Dept. of Atmospheric Science, 1371 Campus Delivery, Fort Collins, CO 80523-1371; e-mail: ejames@atmos.colostate.edu

2.2. *Case Analysis*

Once a list of MCV cases has been compiled, a detailed analysis of each case is carried out based on data from the OM (five-minute observations) and the NOAA Profiler Network (NPN; hourly observations). The OM surface pressure variable is modified by adjusting to a constant elevation of 356.6 m (the mean elevation of all OM stations) and subtracting the mean diurnal pressure signal during the calendar month of interest. In addition, virtual temperature observations from NPN stations equipped with a Radio Acoustic Sounding System (RASS) are linearly interpolated to 25-hPa pressure increments in the vertical, and then linearly interpolated in time, to diminish the extent of missing data. Virtual temperature anomalies are calculated by subtracting the mean virtual temperature from the instantaneous observation at each height; the mean is taken over the period during which the MCV (or its parent MCS) is in Oklahoma.

Observations are augmented in the vicinity of each MCV by means of a time-space transformation (Fujita 1951). OM (NPN) observations taken five and ten minutes (one hour) before and after each time are "transformed" from time to space, and plotted along the direction of motion of the MCV. The MCV heading and speed are determined based on level 3 radar imagery from individual Weather Surveillance Radar-1988 Doppler (WSR-88D) stations in Oklahoma. The transformation is applied over a 3º latitude by 3º longitude box centered on the MCV. The size of the box was determined by trial and error, guided by the fact that an MCV might be expected to influence its environment out to a Rossby radius of deformation (about 280 km in a typical MCS environment; Chen and Frank 1993).

Based on these augmented data, detailed analyses of each case are carried out for the period during which the MCV (or its parent MCS) is within the state of Oklahoma. The analyses are undertaken using multiquadratic interpolation (Nuss and Titley 1994) on a 0.1º latitude-longitude grid. The multiquadratic parameter is set to 1.5; the smoothing parameter is set to 5×10^{-6} for OM analyses, and 1×10^{-4} for NPN analyses. These values, determined by trial and error, were found to result in the most realistic analyses.

2.3. *MCV Classification*

Classification of the MCV cases into distinct types is undertaken based on the behavior of the precipitation structure and the surface pressure field in each case. The precipitation structure of each MCV could be followed throughout its life cycle by means of the national network of WSR-88Ds. However, the surface pressure structure of each case could only be determined when the MCV was in the domain of the OM (the state of Oklahoma).

3. RESULTS

This section describes each of the three MCV types producing surface mesolows, in order of their frequency. Two categories of MCV not producing surface mesolows are not discussed in detail. For each type, we present a description of one representative MCV that we observed during our study period, highlighting the unique aspects of that MCV type.

3.1. *Rear-Inflow-Jet MCV*

The most common type of MCV producing a surface mesolow is referred to as the "rear-inflow-jet MCV". This type of MCV comprises 19 (42%) of the cases. A one-tailed student's *t* test reveals that the mean midlevel relative vorticity of rear-inflow-jet MCVs is larger than the mean of the total MCV population; this difference is significant at the 99% level.

The MCV of 24-25 May 2003, occurring during the Bow Echo and MCV Experiment (BAMEX; Davis et al. 2004) campaign, is described in detail here as a representative case of this type of MCV. The parent MCS develops within southeasterly low-level flow, north of a weak low-level jet. The system forms just downstream of an upper-level ridge, consistent with the findings of Bartels and Maddox (1991). Figure 1a shows the composite radar reflectivity, surface pressure, and observed 10-m winds at 1400 UTC.

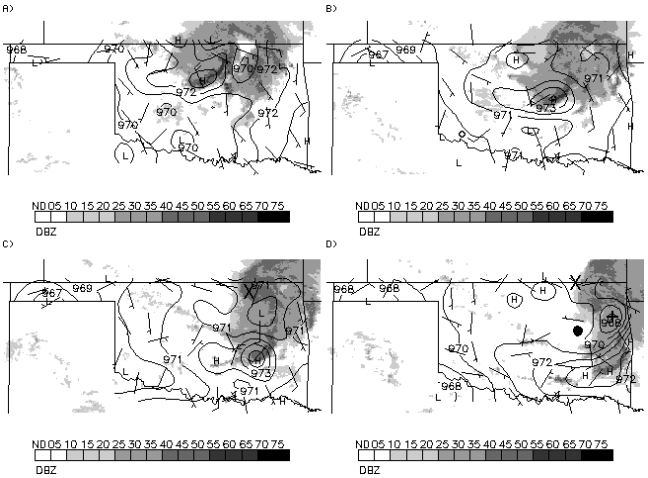

Figure 1: OM surface pressure analyses (hPa; contour interval 1 hPa) overlaid on OM observed 10-m wind barbs (short barb 2.5 m s^{-1}; long barb 5 m s^{-1}) and WSR-88D composite radar reflectivity (dBZ; shaded, with scale at bottom) at (a) 1400, (b) 1500, (c) 1600, and (d) 1700 UTC 24 May 2003. Pressure is adjusted to 356.6 m elevation. Midlevel MCV center, as detected by RUC algorithm, is marked by a large cross in (c)-(d). Tahlequah OM station is marked by a plus sign in (d). Haskell NPN station is marked by a filled circle in (d). "H" and "L" indicate centers of high and low pressure, respectively.

There is extensive stratiform rain in northeastern Oklahoma and southeastern Kansas, while on the southwestern side of this there is a small but intense band of convection oriented northeast-southwest. At the surface, there is a well-defined mesohigh on the southwestern end of this convective line. An hour later, at 1500 UTC (Fig. 1b), the convective line has continued to surge southeastward on the western side of the large stratiform region. The reflectivity field shows a developing rear inflow notch to the north of the convection, suggesting that a strong RIJ is impinging on the back edge of the stratiform region. The surface pressure field is relatively flat within the MCS, with the exception of the mesohigh at the southwestern end of the convective line. At 1600 UTC (Fig. 1c), the associated MCV is first detected by the objective algorithm; its location is marked with a cross. By this time, the convection is becoming weaker, while the stratiform region is taking on cyclonic curvature. South of the MCV, within the stratiform region, a weak mesolow has appeared. By 1700 UTC (Fig. 1d), the mesolow has become concentrated and deep. The stratiform region appears to be eroded on its back edge to the south of the MCV, and the mesolow is located near the apex of this rear inflow notch.

Figure 2 (a and b) shows a meteogram for the Tahlequah OM station (location shown in Fig. 1d). The

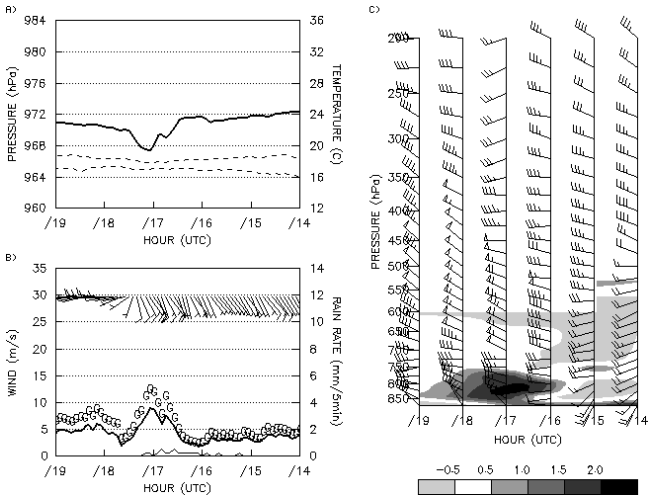

Figure 2: (a and b) Meteogram for Tahlequah OM station (location marked in Fig. 1d) and (c) observed time-height section for Haskell NPN station (location marked in Fig. 1d), 1400-1900 UTC 24 May 2003. Time runs from left to right. Parameters displayed are (a) surface pressure (hPa; solid line; left axis) adjusted to 356.6 m elevation and 1.5-m air temperature and dewpoint temperature (ºC; dashed lines; right axis); (b) observed 10-m wind barbs (short barb 2.5 m s^{-1}; long barb 5 m s^{-1}), wind speed (m s^{-1}; thick solid line; left axis), wind gusts (m s^{-1}; "G"; left axis), and rainfall (mm $(5\ min)^{-1}$; thin solid line; right axis); and (c) horizontal wind (short barb 2.5 m s^{-1}; long barb 5 m s^{-1}; flag 25 m s^{-1}) and RASS virtual temperature anomalies (ºC; shaded, with scale at bottom).

pressure trace shows a very strong and sharp mesolow passing the station at 1705 UTC. The 1.5-m temperature and dewpoint remain nearly constant and quite close together, indicating high relative humidity. If the mesolow is a hydrostatic phenomenon, as will be argued, the associated temperature perturbations must be confined to regions above the surface. The mesolow passes the station at the same time as the cessation of stratiform rainfall, as noted in several other studies (Johnson and Hamilton 1988; Stumpf et al. 1991).

This case appears very similar to the OK PRE-STORM MCV of 6-7 May 1985, as described by Brandes (1990). That case involved a strong RIJ on the south side of the MCV, leading to a rear inflow notch with a pronounced surface mesolow at its apex.

To explain the observed surface pressure features on 24 May 2003 it is necessary to examine observations aloft. Figure 2c shows a time-height section of observations from the Haskell NPN station (location shown in Fig. 1d). The feature of interest is the pronounced low-level virtual warming that occurs over Haskell at 1700 UTC. The virtual temperature anomaly reaches a peak of 2.24 ºC at 825 hPa; positive anomalies extend up to 750 hPa. This sharp low-level warming is evidently a manifestation of strong subsidence warming associated with a descending RIJ at the back edge of the stratiform precipitation shield. The wind profile at Haskell supports this, with the warming occurring at the base of strong west-northwesterly flow (50 kts [26 m s^{-1}] at 700 hPa). Note that the core of the jet rises from 600 to 500 hPa during 1700 to 1900 UTC, consistent with fixed-point observations of a descending jet in an eastward-moving system. Calculation of the hydrostatic pressure change associated with the warming in the Haskell virtual temperature profile from 1500 to 1700 UTC yields a value of -0.87 hPa. The observed change at Okmulgee, the closest OM station to the Haskell NPN site, over this same time period is -0.79 hPa, suggesting that the low-level warming can explain the entirety of the pressure drop. The significantly larger pressure fall observed at Tahlequah (-3.62 hPa) over this same period suggests that the Haskell profiler did not sample the core of the low-level warming (see Fig. 3).

This MCV was the focus of Intensive Observing Period (IOP) 1 during the BAMEX campaign, and dense aircraft observations were taken during the afternoon of 24 May (Davis and Trier 2007). Figure 3 shows their east-west cross-sections of the system, constructed from dropsonde observations and valid at 1930 UTC. The dropsonde observations show a very similar virtual temperature structure to the NPN observations, including a concentrated warm anomaly of more than 3 ºC centered near 850 hPa. The virtual warmth extends up to 600 hPa and then transitions to a cold anomaly, as in the NPN observations. Also, similar to the NPN observations, a region of virtually

cool air is seen a few hundred km to the east of the warm anomaly, extending over a deep layer except for a small warm pocket near 700 hPa. The extent of the agreement between the two independent datasets is remarkable, and provides confidence in the thermal structure of this MCV. These observations suggest that, in these rear-inflow-jet MCVs, many of which display similar structure (not shown), the small but intense surface mesolow is a reflection of concentrated low-level subsidence warming occurring within a RIJ.

3.2. *Collapsing-Stratiform-Region MCV*

The second type of mesolow-producing MCV observed is termed the "collapsing-stratiform-region MCV", due to the apparent role of the dissipating stratiform region in the development of both the midlevel vortex and a surface mesolow. Eight of these cases are observed during the period of study (18% of the total). The mean radius of collapsing-stratiform-region MCVs is smaller than that of the total MCV population; this difference is significant at the 90% level. Similarly, the mean midlevel relative vorticity within collapsing-stratiform-region MCVs is less than the mean of the entire MCV population; this difference is significant at the 95% level. The reduced radius and intensity of these MCVs is likely related to the small size of the parent MCSs; these MCSs are anomalously small even at maturity.

The typical evolution of collapsing-stratiform-region MCVs is illustrated with one of the cases documented here, occurring on 9-10 August 2004. This MCV forms from a southward-moving MCS within northwesterly upper-level flow and weak low- and midlevel flow, once again in proximity to an upper-level ridge (Bartels and Maddox 1991). Figure 4a shows the parent MCS at 0800 UTC, as it enters northwestern Oklahoma. The radar reflectivity shows a stratiform region centered just north of the Kansas-Oklahoma border, with a mesohigh at the southern fringe of the precipitation. An hour later (Fig. 4b), the stratiform region is in the process of dissipating, and the mesohigh has moved farther south, while a pronounced pressure gradient is beginning to appear within the southern portion of the dissipating precipitation shield. By 1000 UTC (Fig. 4c), the mesohigh is centered south of the remaining rain area, and a broad mesolow has developed to its north. The MCV associated with the system is first detected by the objective algorithm at this time, located directly over the southern portion of the mesolow. By 1100 UTC (Fig. 4d), the stratiform precipitation has nearly dissipated, leaving a large and relatively deep mesolow centered in northern Oklahoma and a weakening mesohigh to its south.

Figure 5 (a and b) shows a meteogram for the Breckinridge OM station (location marked in Fig. 4d). The pressure trace shows the passage of a well-defined mesolow of 4-hPa amplitude, lasting 3 h with a minimum pressure near 1100 UTC. While the magnitude of the pressure gradient between the mesohigh and mesolow is fairly significant (6 hPa (100 km)$^{-1}$), the observed winds at the surrounding OM stations remain quite low. This is presumably due to

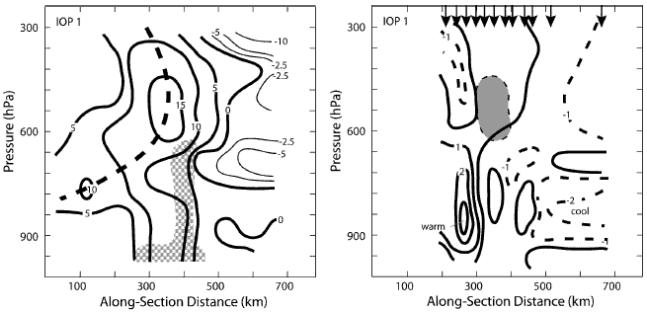

Figure 3: East-west cross section of BAMEX IOP 1 MCV at 1930 UTC 24 May 2003. Left panel displays relative vorticity (10^{-5} s^{-1}; contour interval 5×10^{-5} s^{-1} for positive values, 2.5×10^{-5} s^{-1} for negative values), with gray stippling indicating regions where the standard deviation of vorticity exceeds half the maximum value (see details in Davis and Trier 2007), and the heavy dashed line indicating vortex axis. Right panel displays virtual potential temperature deviations (K; contour interval 1 K), with gray shading indicating relative vorticity greater than 1.5×10^{-4} s^{-1}, and arrows indicating the locations of soundings projected onto the cross section. From Davis and Trier (2007).

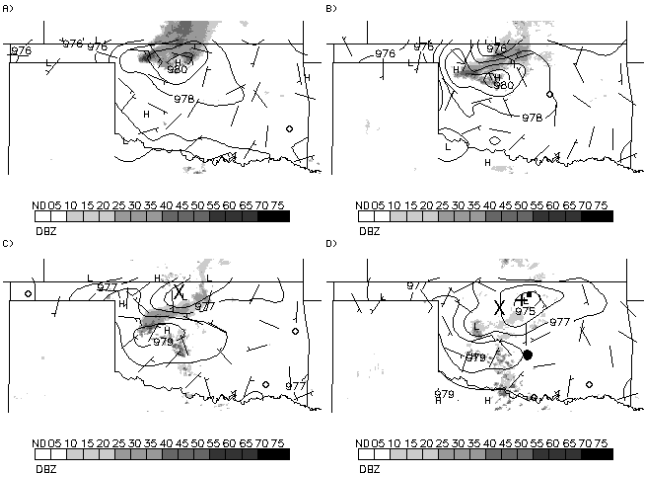

Figure 4: OM surface pressure analyses (hPa; contour interval 1 hPa) overlaid on OM observed 10-m wind barbs (short barb 2.5 m s^{-1}; long barb 5 m s^{-1}) and WSR-88D composite radar reflectivity (dBZ; shaded, with scale at bottom) at (a) 0800, (b) 0900, (c) 1000, and (d) 1100 UTC 9 Aug 2004. Pressure is adjusted to 356.6 m elevation. Midlevel MCV center, as detected by RUC algorithm, is marked by a large cross in (c)-(d). Breckinridge OM station is marked by a plus sign in (d). Purcell NPN station is marked by a filled circle in (d). ARM site is marked by a filled square in (d). "H" and "L" indicate centers of high and low pressure, respectively.

the transient and unbalanced nature of the pressure field (Vescio and Johnson 1992). Another notable feature of Fig. 5a is the minimal temperature and dewpoint variations during the passage of the mesolow. The evolution of the 9-10 August 2004 case appears very similar to that of the 23-24 June 1985 OK PRE-STORM MCS, examined by Johnson et al. (1989).

Once again, in order to investigate the causes of the surface pressure features associated with collapsing-stratiform-region MCVs, it is necessary to look above the surface. Fig. 5c shows a time series of observations from the Purcell NPN station (location marked in Fig. 4d) during the 9-10 August 2004 case. Note that the Purcell station is located in south-central Oklahoma; thus the mesolow does not move overhead until 1300 UTC, and is weaker by this time (not shown). Around the same time as mesolow passage, the RASS virtual temperature anomalies exhibit a broad and deep maximum. The warm anomaly extends from 850 hPa to near the top of the RASS measurements (575 hPa). The anomaly lasts several hours, and reaches a maximum of 1.88 ºC. Direct calculation of the hydrostatic pressure change associated with the change in the RASS virtual temperature profile from 1100 to 1300 UTC below 600 hPa gives a value of -1.75 hPa. The observed pressure drop at Washington, the nearest OM station to Purcell, is 1.52 hPa over the same two-hour period. This suggests (assuming no compensating warming aloft) that the warming observed below 600 hPa can explain the entirety of the pressure fall.

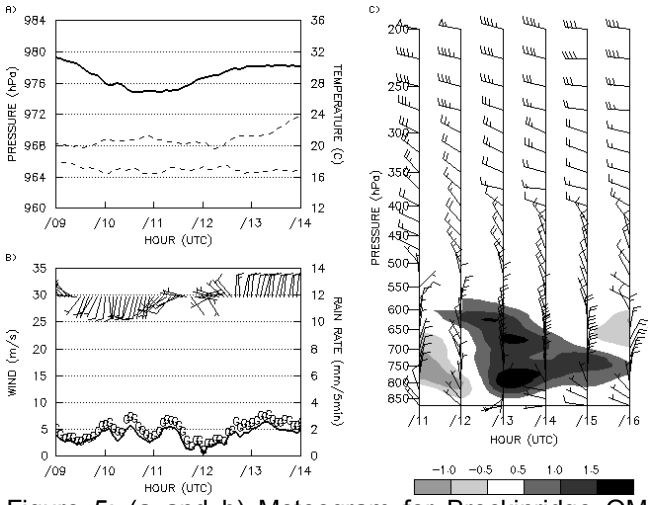

Figure 5: (a and b) Meteogram for Breckinridge OM station (location marked in Fig. 4d), 0900-1400 UTC, and (c) observed time-height section for Purcell NPN station (location marked in Fig. 4d), 1100-1600 UTC 9 Aug 2004. Time runs from left to right. Parameters displayed are (a) surface pressure (hPa; solid line; left axis) adjusted to 356.6 m elevation and 1.5-m air temperature and dewpoint temperature (ºC; dashed lines; right axis); (b) observed 10-m wind barbs (short barb 2.5 m s^{-1}; long barb 5 m s^{-1}), wind speed (m s^{-1}; thick solid line; left axis), wind gusts (m s^{-1}; "G"; left axis), and rainfall (mm (5 min)$^{-1}$); thin solid line; right axis); and (c) horizontal wind (short barb 2.5 m s^{-1}; long barb 5 m s^{-1}; flag 25 m s^{-1}) and RASS virtual temperature anomalies (ºC; shaded, with scale at bottom).

It seems probable that this virtual warmth is a result of broad subsidence warming, which could occur within the dissipating remnants of an MCS. After the dissipation of all the precipitation within the MCS stratiform region, continuing descent would produce adiabatic warming within a stably stratified atmosphere. Support for this hypothesis is presented in Fig. 6, which shows a skew *T*-log *p* diagram of a radiosonde launched from the Atmospheric Radiation Measurement (ARM) site in northern Oklahoma (location shown in Fig. 4d) at 1136 UTC. Above a low-level nocturnal inversion, there is a deep dry-adiabatic layer up to above 700 hPa. This dry-adiabatic layer resembles the "onion" soundings documented by Zipser (1977) in the trailing stratiform regions of tropical MCSs. At this time of day, this layer likely represents a region of subsidence warming, especially considering the absence of any such well-mixed layer in the 1200 UTC soundings at Norman, Dodge City, or Amarillo.

Taken together, these observations strongly suggest that the well-defined mesolows observed in collapsing-stratiform-region MCVs are due to broad low- to midlevel subsidence warming occurring within the dissipating stratiform regions of MCSs. The frequent close proximity of the surface mesolow and midlevel vortex suggests there could be a dynamical link between the two. From the perspective of the vorticity equation, low- to midlevel subsidence, such as that producing the mesolows in these systems, would contribute to a spinup of vorticity by the stretching term. In a favorable environment of weak cyclonic

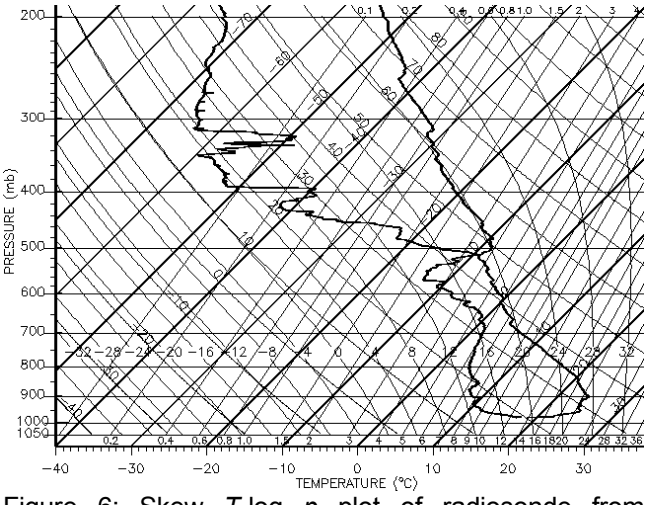

Figure 6: Skew *T*-log *p* plot of radiosonde from Oklahoma ARM site (location marked in Fig. 4d) at 1136 UTC 9 Aug 2004. Right-hand trace is temperature (ºC), and left-hand trace is dewpoint temperature (ºC).

vorticity, this contribution could be a major factor in MCV formation and amplification at low levels.

3.3. Vertically-coherent MCV

The third kind of MCV producing a surface mesolow is termed the "vertically-coherent MCV". Only one of the cases documented here displays this behavior: that of 29 July 2004. This appears to be the only case where the midlevel vortex produces a genuine reflection in the surface wind field (i.e., an associated low-level vortex). This MCV has a larger radius than the mean of the total population.

The MCV forms in a rather moist environment in northern Texas, just ahead of a mid- to upper-level shortwave trough and north of a LLJ. The flow configuration in this case differs from the archetypal pattern of MCV formation within an upper-level ridge. The distinguishing feature of this MCV is the persistent and relatively large-scale surface mesolow attendant to the midlevel circulation. Fig. 7a shows the precipitation structure and surface pressure field at 1300 UTC on 29 July 2004. The midlevel MCV center is just south of the analysis domain at this time. There is widespread light to moderate stratiform precipitation within the MCV's circulation. The pressure field shows a large and broad mesolow just southwest of the precipitation shield. An hour later (Fig. 7b), the mesolow has consolidated, and the entire rain shield is rotating cyclonically around the mesolow; this rotation is clearly seen when successive 15-min radar images are animated on the computer screen. During 1500-1600 UTC (Fig. 7c,d), the system continues to drift slowly northeastward through Oklahoma, with the mesolow remaining strong. It should be noted that, throughout the analysis period, the observed surface winds, although light, form a closed cyclonic circulation centered on the mesolow.

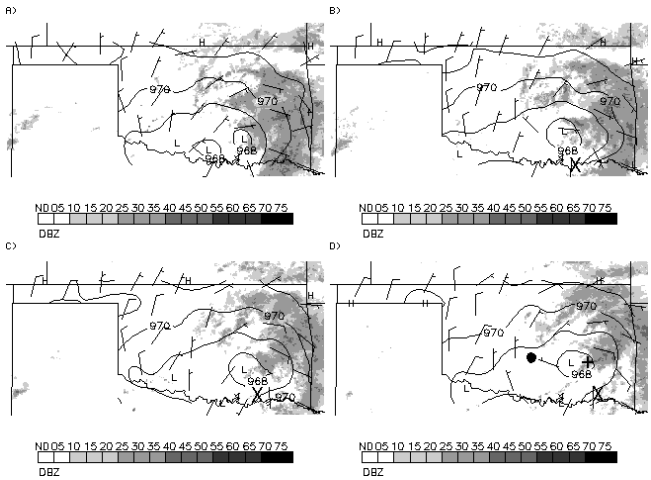

Figure 7: OM surface pressure analyses (hPa; contour interval 1 hPa) overlaid on OM observed 10-m wind barbs (short barb 2.5 m s^{-1}; long barb 5 m s^{-1}) and WSR-88D composite radar reflectivity (dBZ; shaded, with scale at bottom) at (a) 1300, (b) 1400, (c) 1500, and (d) 1600 UTC 29 Jul 2004. Pressure is adjusted to 356.6 m elevation. Midlevel MCV center, as detected by RUC algorithm, is marked by a large cross in (b)-(d). McAlester OM station is marked by a plus sign in (d). Purcell NPN station is marked by a filled circle in (d). "H" and "L" indicate centers of high and low pressure, respectively.

The surface weather effects of this MCV can be seen in the meteogram for the OM station at McAlester (location shown in Fig. 7d), displayed in Fig. 8a,b. The pressure trace reveals that the mesolow is very broad and shallow; the pressure fall is only about 2 hPa, but commences hours before the lowest pressure is observed (1630 UTC). The near-surface air is very nearly saturated, with dewpoint depressions of <1 ºC much of the time. The MCV occurs within a north-south temperature gradient, with the temperature rising 4 ºC over 2 h; this temperature gradient seems to be associated with a weak surface warm front. While the winds clearly show the passage of a cyclonic circulation near 1630 UTC, the speeds remain generally below 5 m s^{-1}.

Figure 8c shows a time-height section of NPN observations from the station at Purcell (location shown in Fig. 7d). The weakness of the virtual temperature anomalies in this case is notable; the warmest anomaly

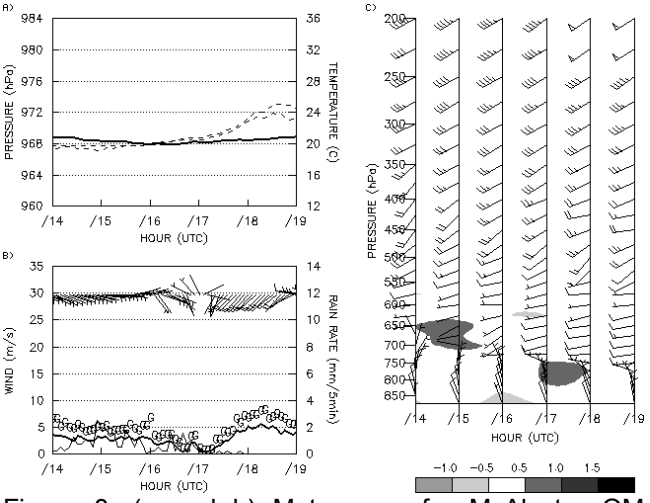

Figure 8: (a and b) Meteogram for McAlester OM station (location marked in Fig. 7d) and (c) observed time-height section for Purcell NPN station (location marked in Fig. 7d), 1400-1900 UTC 29 Jul 2004. Time runs from left to right. Parameters displayed are (a) surface pressure (hPa; solid line; left axis) adjusted to 356.6 m elevation and 1.5-m air temperature and dewpoint temperature (ºC; dashed lines; right axis); (b) observed 10-m wind barbs (short barb 2.5 m s^{-1}; long barb 5 m s^{-1}), wind speed (m s^{-1}; thick solid line; left axis), wind gusts (m s^{-1}; "G"; left axis), and rainfall (mm $(5\ min)^{-1}$; thin solid line; right axis); and (c) horizontal wind (short barb 2.5 m s^{-1}; long barb 5 m s^{-1}; flag 25 m s^{-1}) and RASS virtual temperature anomalies (ºC; shaded, with scale at bottom).

observed is only 0.7 ºC (650 hPa, 1500 UTC). Figure 9 shows a north-south cross section of PV through the MCV center at 1200 UTC, based on the RUC analysis. The MCV is represented as a large and relatively deep PV tower, nearly vertically aligned. The PV tower appears directly over the surface mesolow (location marked in Fig. 9), which is itself embedded within the surface frontal zone. PV of >10^{-6} K m^2 kg s^{-1} extends up to nearly 450 hPa, and the PV tower is about 200 km in diameter. The isentropes, overlaid on the PV field in Fig. 9, are slightly depressed within the PV tower from 800 to 500 hPa; this warm core does not appear to penetrate to the surface. There is no negative PV anomaly overlying the PV tower as has been reported in other MCVs (e.g., Fritsch et al. 1994).

An examination of the BAMEX MCV cases discussed by Davis and Trier (2007) reveals a very similar MCV to the present case, occurring during IOP 8 on 11 June 2003. Figure 10 shows east-west cross sections of this MCV, in terms of relative vorticity and virtual potential temperature anomaly. The relative vorticity cross section shows a coherent and vertically stacked vortex, with strong vorticity (>1.5x10^{-4} s^{-1}) extending up to 400 hPa. While relative vorticity is not equivalent to PV, the shape and depth of the relative vorticity maximum is remarkably similar to the PV tower seen in the 29 July 2004 case (Fig. 9). Another similarity emerges in the right-hand panel of Fig. 10, which shows that the virtual potential temperature deviations in the vicinity of this BAMEX MCV are minimal. The occurrence of such an MCV during the BAMEX campaign, displaying such marked similarities to the case documented here, supports the classification of these MCVs in their own category.

The question arises as to what mechanism is responsible for the development of low pressure at the surface in vertically coherent MCVs. The vertical coherence of the PV anomaly in these cases, as well as the proximity of the surface mesolow to the center of the PV tower, suggests that the mesolow may be due to a developing, deep warm core within the MCV. Such a warm core could be produced by the diabatic heating occurring within the persistent precipitation shield in the vicinity of the MCV. In the 29 July 2004 case, the precipitation shield itself, occurring on the east side of the vortex, is likely due to the balanced lifting mechanism proposed by Raymond and Jiang (1990) acting on the north-south temperature gradient associated with the warm front. The extension of the MCV to the surface in these cases is likely enabled by the relative lack of a surface-based cold pool due to the very moist environment; according to the RUC analyses, the precipitable water in the vicinity of the vortex remains well above 5 cm (not shown). This mechanism of surface low development due to the strengthening and deepening of a warm core has been documented in prior studies of MCVs (Fritsch et al. 1994; Rogers and Fritsch 2001; Trier and Davis 2002; Davis and Galarneau 2009). The low-level cyclonic vorticity maximum would develop in response to the presence of a surface mesolow.

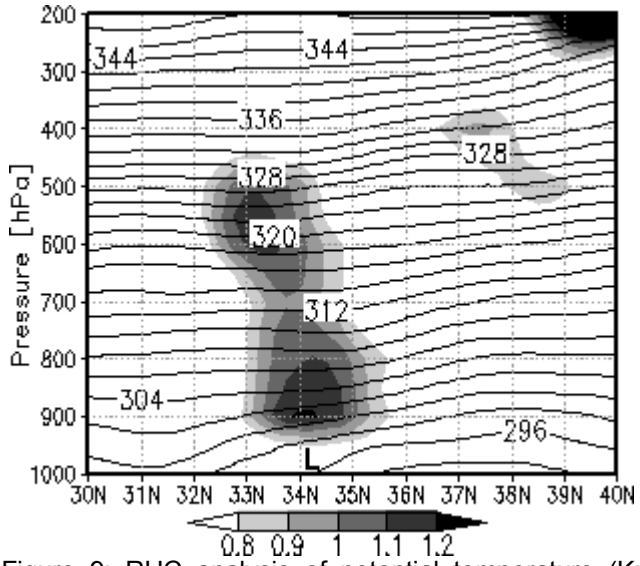

Figure 9: RUC analysis of potential temperature (K; contour interval 2 K) and PV (10^{-6} K m^2 kg^{-1} s^{-1}; shaded, with scale at bottom) along vertical section at 96.75ºW at 1200 UTC 29 July 2004. Mesolow location is marked by "L" on the lower axis.

4. DISCUSSION

This study classifies MCVs into several types involving recurring patterns of organization and surface effects. The majority of the MCVs documented herein develop within generally weak midlevel flow in proximity to an upper-level ridge, consistent with the characteristic MCV flow environment identified by Bartels and Maddox (1991). The remainder of this

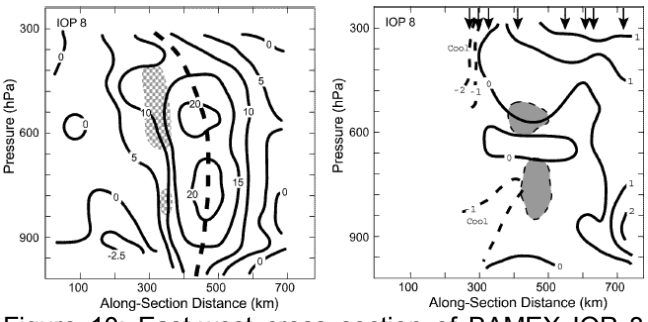

Figure 10: East-west cross section of BAMEX IOP 8 MCV at 1730 UTC 11 Jun 2003. Left panel displays relative vorticity (10^{-5} s^{-1}; contour interval 5x10^{-5} s^{-1} for positive values, 2.5x10^{-5} s^{-1} for negative values), with gray stippling indicating regions where the standard deviation of vorticity exceeds half the maximum value (see details in Davis and Trier 2007), and the heavy dashed line indicating vortex axis. Right panel displays virtual potential temperature deviations (K; contour interval 1 K), with gray shading indicating relative vorticity greater than 2x10^{-4} s^{-1}. From Davis and Trier (2007).

section summarizes the five types, and presents conceptual models of two of the three MCV types containing significant surface mesolows. Only one vertically-coherent MCV was observed; thus, despite its many interesting features and potential relevance to tropical cyclogenesis, we do not attempt to develop a conceptual model of this MCV type.

Rear-inflow-jet MCVs (19 of the 45 cases, or 42% of the total) are the most frequent MCV type containing a marked surface mesolow. In these cases, the development of low surface pressure seems to occur due to the well-documented wake low mechanism, whereby a RIJ flowing into an MCS stratiform region descends strongly, producing a concentrated region of subsidence warming at low levels where the precipitation has evaporated (Johnson and Hamilton 1988). Figure 11 shows a conceptual diagram of the evolution of these MCVs. The left panel represents the mature stage of the parent MCS. These MCSs show a variety of organizations, but one of the most frequent is the leading-line/trailing-stratiform MCS (Houze et al. 1990). The surface pressure field at this time consists of a broad mesohigh within the precipitation. The middle panel of Fig. 11 shows a later stage of development; by this time, the precipitation structure is starting to develop asymmetry, with the right-hand portion of the stratiform region (relative to system motion) eroding due to the development of rear inflow on this side of the incipient MCV. A small mesolow appears behind this eroded portion of the stratiform region. On average, the MCV is first detected by the objective algorithm near this time. The specific location of the MCS mesohigh varies considerably among the cases, but in the mean the highest pressure is located in the left-hand portion of the precipitation region relative to system motion. At the final stage, depicted in the right-hand panel of Fig. 11, the stratiform region has been largely shunted to the left of the system motion. The MCV is intensifying in the remaining portion of the stratiform region, and a concentrated and intense mesolow has formed just behind the eroded portion of the stratiform region.

The organization of many of these rear-inflow-jet MCVs (and, to a lesser extent, that of the collapsing-stratiform-region MCVs) strongly resembles an asymmetric squall line (Houze et al. 1990), but with an embedded MCV in the northern portion of the system, as introduced by Houze et al. (1989, their Fig. 2b). A similar asymmetric precipitation structure has been documented among the OK PRE-STORM MCSs by Loehrer and Johnson (1995; see their Fig. 22b), but with a mesolow occurring behind the trailing stratiform region on the north side of the system rather than on the south side. Mesolows do occur in this position in two of the MCVs examined here; these MCVs are classified as rear-inflow-jet MCVs due to the positioning of the mesolow just behind the stratiform precipitation. This subset of rear-inflow-jet MCVs may have distinct features, and merits further study.

The role of the MCV in these rear-inflow-jet MCVs is somewhat obscure; perhaps it influences the positioning and strength of the rear inflow. Brandes (1990) argued that the MCV within the 6-7 May 1985 OK PRE-STORM MCS enhanced the rear inflow on its southern side; this MCV displayed many similarities to the rear-inflow-jet MCVs described here. In that case, as well as in the cases documented here, the location of the mesolow appears to be determined by the location of the RIJ with respect to the stratiform region.

The eight collapsing-stratiform-region MCVs (18% of the MCVs) display the least variation in structure of all the MCV types. Figure 12 shows a conceptual model of the evolution of the collapsing-stratiform-region MCV. The left panel represents the

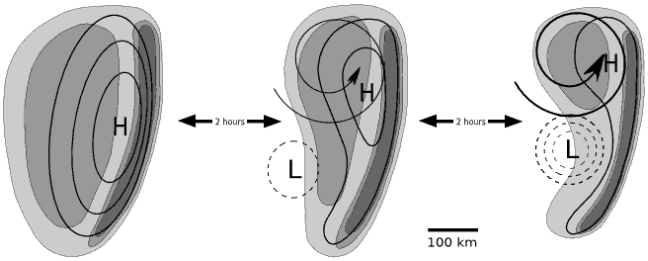

Figure 11: Conceptual model of the typical evolution of a rear-inflow-jet MCV. Time runs from left to right, and evolution is with respect to a system moving towards the right. Shading represents composite radar reflectivity; light shading indicates 30-40 dBZ, moderate shading indicates 40-50 dBZ, and dark shading indicates >50 dBZ. Thin black lines represent isobars of surface pressure (contour interval 1 hPa; negative contours dashed). “H” indicates center of mesohigh, and “L” indicates center of mesolow. Spiral indicates location of developing midlevel vortex, with line thickness proportional to vortex intensity.

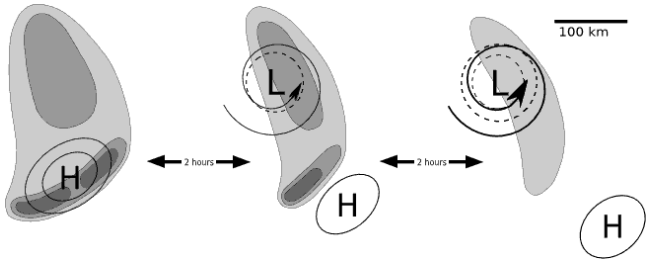

Figure 12: Conceptual model of the typical evolution of a collapsing-stratiform-region MCV. Time runs from left to right, and evolution is with respect to a system moving towards the right. Shading represents composite radar reflectivity; light shading indicates 30-40 dBZ, moderate shading indicates 40-50 dBZ, and dark shading indicates >50 dBZ. Thin black lines represent isobars of surface pressure (contour interval 1 hPa; negative contours dashed). “H” indicates center of mesohigh, and “L” indicates center of mesolow. Spiral indicates location of developing midlevel vortex, with line thickness proportional to vortex intensity.

mature stage of the parent MCS; these MCSs often display a very specific organization consisting of a weak convective line (variably oriented, but on average shifted 45º relative to the direction of motion) with a small stratiform region to the left of the system motion. This is similar to the "parallel stratiform" organization of Parker and Johnson (2000), but the convection is not always linear or oriented perpendicular to system motion. At this stage, the surface pressure field is characterized by a mesohigh within the convective region. The central panel of Fig. 12 shows an intermediate stage in the evolution of the system, by which time the convection is weakening, the stratiform region is beginning to dissipate, a small mesolow appears at the rear of the stratiform region, and the surface mesohigh is beginning to move out ahead of the precipitation and weaken. The midlevel vortex generally becomes sufficiently intense to be first detected by the objective algorithm a few hours after this time. The right panel in Fig. 12 shows the final stage in the evolution of these MCVs; the broadening and deepening mesolow has moved into the dissipating remnants of the stratiform region, and the weak mesohigh has moved farther ahead. The formation of both the MCV and the surface mesolow occurs during the weakening stage of the parent MCS.

It was noted in section 3b that collapsing-stratiform-region MCVs tend to be smaller and weaker than other MCVs. These characteristics are a possible explanation for the lack of RIJs and associated wake lows within these MCVs. Regarding the movement of the mesohigh out ahead of the precipitation, similar behavior has recently been observed associated with bowing line segments in linear MCSs (Adams-Selin and Johnson 2009). It is not clear whether the same mechanisms are acting in these collapsing-stratiform-region MCVs. We do note that there is very little temperature perturbation associated with these mesohighs, which suggests a gravity wave mechanism rather than a density current mechanism. The surface mesolow appears at least indirectly related to the development of the MCV; it is likely that both develop as a result of relatively deep low- to midlevel subsidence. This subsidence is driven by the dissipation of the stratiform precipitation and the associated collapsing and spreading of the surface-based cold pool. The compression warming occurring within this subsidence region is responsible, hydrostatically, for the reduced pressure at the surface, and the column stretching implied by the subsidence favors the concentration of midlevel relative vorticity. This sequence of events was suggested by Johnson et al. (1989) as an explanation for the surface observations obtained in the 23-24 June 1985 OK PRE-STORM MCS, which clearly contained a collapsing-stratiform-region MCV.

The vertically-coherent MCV observed in this study, on 29 July 2004, has several unique characteristics compared with the other MCV types. The breadth and persistence of the mesolow suggests that different dynamics are active than in the other cases. Upper-air observations from the NPN do not reveal any obvious low-level warming such as would be expected in the vicinity of MCVs of the first two types. However, analyses from the RUC do indicate a relatively deep warm core at the mid levels, associated with a coherent tower of high PV. The surface mesolow is apparently a hydrostatic result of the mesoscale warm core associated with the MCV. It is not immediately obvious why the warm core is so much deeper in this case than in other cases; perhaps it is related to the longevity of the precipitation shield and its associated diabatic heating. While the warm core does not appear to extend to the surface, it is also apparent that there is no well-defined surface cold pool. The weakness of the cold pool may be the defining feature allowing such a strong mesolow to form. Vertically-coherent MCVs have recently been simulated by Conzemius et al. (2007) and Davis and Galarneau (2009); these authors emphasize the role of low-level convergence within a moist neutral environment in the development of a surface cyclonic circulation. We are unable to definitively determine the mechanisms responsible for the development of surface features in the 29 July 2004 MCV, because the vortex acquires a well-defined surface circulation and mesolow before moving into Oklahoma.

It is tempting to compare the vertically-coherent MCV with an incipient tropical cyclone. The similarities are considerable: there is a closed surface circulation with a well-defined low pressure center, a large and deep tower of high PV extending into the mid to upper troposphere, and an extremely moist environment. The lack of any significant organization of the precipitation field, as well as the weakness of the surface wind field, may be related to the fact that the system is in its early stages of development. Soundings taken in the environment of the 29 July 2004 MCV (not shown) reveal that the atmosphere is nearly saturated, with a near moist-adiabatic lapse rate. The lack of strong surface fluxes from an underlying warm ocean explains the failure of tropical cyclogenesis (Fritsch et al. 1994); such fluxes would likely allow the MCV to transition to a true tropical cyclone (Rogers and Fritsch 2001) given weak vertical wind shear. Past studies (e.g., Bosart and Sanders 1981) have reported tropical cyclogenesis from MCVs.

The final two types of MCVs documented in this study represent vortices which fail to develop significant mesolows. The mesolow development mechanisms active in the previous cases are not present in these MCVs for several possible reasons. The remnant-circulation MCVs (14 cases, or 31% of the total) lack significant precipitation in their vicinity; precipitation is required for the hypothesized mesolow development mechanisms active in the other MCV types. The cold-pool-dominated MCVs (three cases, or 7% of the total) contain significant precipitation, but it is

likely that the deep and extensive surface cold pools mask any potential pressure perturbations due to warming aloft.

The limited extent of our study domain should be kept in mind when considering these results. More than half of the 45 MCVs documented here moved outside of Oklahoma at some point during their life cycle; during these times the surface pressure field associated with the vortices is unknown. This limitation, as well as deficiencies in the RUC model, introduces some uncertainty into the classifications. Oklahoma is only a fraction of the area frequented by MCVs in the USA, but it is likely representative. Thus, we expect our MCV classifications to hold in other portions of the central USA.

5. CONCLUSIONS

This study has described the precipitation structure and evolution of midlatitude MCVs observed over the state of Oklahoma during four years. MCV case detection was achieved with an objective algorithm developed to operate on analyses from the operational RUC model, as described by DAT. Five repeating patterns of precipitation structure and surface pressure evolution have been defined, three of which produce well-defined surface mesolows.

Several characteristics of the MCV types have potential utility for forecasters. The behavior of rear-inflow-jet MCVs implies that the detection of an MCV within a large and vigorous MCS could alert forecasters to the possibility of wake low development and the associated aviation hazard of low-level wind shear (Johnson 2001). Similarly, the evolution of collapsing-stratiform-region MCVs suggests that forecasters should be vigilant for MCV development, which may influence convective potential in the region over the next 24 h, when a broad and deep mesolow forms within the collapsing stratiform region of an MCS. Vertically-coherent MCVs should be closely monitored in coastal regions during the hurricane season, as they can undergo tropical cyclogenesis over a warm ocean surface (Bosart and Sanders 1981). Extratropical cyclogenesis can also occur from MCVs (Zhang and Harvey 1995), although this is perhaps a less significant threat due to the weak ambient temperature gradients during the warm season.

Several avenues of future research are suggested by the findings of this study. Further observations of MCVs are needed; specifically, high-resolution upper-air observations, such as can be obtained with dropsonde-equipped aircraft during field campaigns, would be helpful in diagnosing the detailed structure of MCVs. Numerical simulations of MCV evolution in a variety of environments could confirm the mesolow formation mechanisms proposed in this study. In addition, such simulations may elucidate the underlying causes for the wide variety of MCV structures and evolutions observed. Finally, the identification of distinct classes of MCV suggests that a composite analysis of each type may be beneficial. It is anticipated that continuing research in this area will eventually lead to marked improvements in warm season forecast skill in the midlatitudes.

REFERENCES

Adams-Selin, R. D., and R. H. Johnson, 2009: Mesoscale surface pressure and temperature features associated with bow echoes. *Mon. Wea. Rev.,* in press.

Bartels, D. L., and R. A. Maddox, 1991: Midlevel cyclonic vortices generated by mesoscale convective systems. *Mon. Wea. Rev.,* 119, 104-118.

Benjamin, S. G., and Coauthors, 2004: An hourly assimilation-forecast cycle: The RUC. *Mon. Wea. Rev.,* 132, 495-518.

Bosart, L. F., and F. Sanders, 1981: The Johnstown flood of July 1977: A long-lived convective system. *J. Atmos. Sci.,* 38, 1616-1642.

Brandes, E. A., 1990: Evolution and structure of the 6-7 May 1985 mesoscale convective system and associated vortex. *Mon. Wea. Rev.,* 118, 109-127.

Chen, S. S., and W. M. Frank, 1993: A numerical study of the genesis of extratropical convective mesovortices. Part I: Evolution and dynamics. *J. Atmos. Sci.,* 50, 2401-2426.

Conzemius, R. J., R. W. Moore, M. T. Montgomery, and C. A. Davis, 2007: Mesoscale convective vortex formation in a weakly sheared moist neutral environment. *J. Atmos. Sci.,* 64, 1443-1466.

Cunning, J. B., 1986: The Oklahoma-Kansas Preliminary Regional Experiment for STORM-Central. *Bull. Amer. Meteor. Soc.,* 67, 1478-1486.

Davis, C. A., and T. J. Galarneau, 2009: The vertical structure of mesoscale convective vortices. *J. Atmos. Sci.,* 66, 686-704.

Davis, C. A., and S. B. Trier, 2007: Mesoscale convective vortices observed during BAMEX. Part I: Kinematic and thermodynamic structure. *Mon. Wea. Rev.,* 135, 2029-2049.

Davis, C. A., D. A. Ahijevych, and S. B. Trier, 2002: Detection and prediction of warm season midtropospheric vortices by the Rapid Update Cycle. *Mon. Wea. Rev.,* 130, 24-42.

Davis, C. A., and Coauthors, 2004: The Bow Echo and MCV Experiment: Observations and opportunities. *Bull. Amer. Meteor. Soc.,* 85, 1075-1093.

Fritsch, J. M., J. D. Murphy, and J. S. Kain, 1994: Warm core vortex amplification over land. *J. Atmos. Sci.,* 51, 1780-1807.

Fujita, T. T., 1951: Microanalytical study of thunder-nose. *Geophys. Mag. Tokyo,* 22, 78-88.

Galarneau, T. J., Jr., L. F. Bosart, C. A. Davis, and R. McTaggart-Cowan, 2009: Baroclinic transition of a long-lived mesoscale convective vortex. *Mon. Wea. Rev.,* 137, 562-584.

Houze, R. A., Jr., B. F. Smull, and P. Dodge, 1990: Mesoscale organization of springtime rainstorms in Oklahoma. *Mon. Wea. Rev.,* 118, 613-654.

Houze, R. A., Jr., S. A. Rutledge, M. I. Biggerstaff, and B. F. Smull, 1989: Interpretation of Doppler weather radar displays of midlatitude mesoscale convective systems. *Bull. Amer. Meteor. Soc.,* 70, 608-619.

Johnson, R. H., 2001: Surface mesohighs and mesolows. *Bull. Amer. Meteor. Soc.,* 82, 13-31.

Johnson, R. H., and P. J. Hamilton, 1988: The relationship of surface pressure features to the precipitation and airflow structure of an intense midlatitude squall line. *Mon. Wea. Rev.,* 116, 1444-1472.

Johnson, R. H., S. Chen, and J. J. Toth, 1989: Circulations associated with a mature-to-decaying midlatitude mesoscale convective system. Part I: Surface features—heat bursts and mesolow development. *Mon Wea. Rev.,* 117, 942-959.

Loehrer, S. M., and R. H. Johnson, 1995: Surface pressure and precipitation life cycle characteristics of PRE-STORM mesoscale convective systems. *Mon. Wea. Rev.,* 123, 600-621.

Nuss, W. A., and D. W. Titley, 1994: Use of multiquadratic interpolation for meteorological objective analysis. *Mon. Wea. Rev.,* 122, 1611-1631.

Parker, M. D., and R. H. Johnson, 2000: Organizational modes of midlatitude mesoscale convective systems. *Mon. Wea. Rev.,* 128, 3413-3436.

Raymond, D. J., and H. Jiang, 1990: A theory for long-lived mesoscale convective systems. *J. Atmos. Sci.,* 47, 3067-3077.

Rogers, R. F., and J. M. Fritsch, 2001: Surface cyclogenesis from convectively driven amplification of midlevel mesoscale convective vortices. *Mon. Wea. Rev.,* 129, 605-637.

Stumpf, G. J., R. H. Johnson, and B. F. Smull, 1991: The wake low in a midlatitude mesoscale convective system having complex convective organization. *Mon. Wea. Rev.,* 119, 134-158.

Trier, S. B., and C. A. Davis, 2002: Influence of balanced motions on heavy precipitation within a long-lived convectively generated vortex. *Mon. Wea. Rev.,* 130, 877-899.

Vescio, M. D., and R. H. Johnson, 1992: The surface-wind response to transient mesoscale pressure fields associated with squall lines. *Mon. Wea. Rev.,* 120, 1837-1850.

Zhang, D.-L., and R. Harvey, 1995: Enhancement of extratropical cyclogenesis by a mesoscale convective system. *Mon. Wea. Rev.,* 52, 1107-1127.

Zipser, E. J., 1977: Mesoscale and convective-scale downdrafts as distinct components of squall-line structure. *Mon. Wea. Rev.,* 105, 1568-1589.